Journal of Alloys and Compounds 658 (2016) 367-371
http://dx.doi.org/10.1016/j.jallcom.2015.10.210

Anisotropy field distribution in soft magnetic Hitperm alloys submitted to different field annealing processes

J. S. Blázquez[1*], J. Marcin[2], F. Andrejka[2], V. Franco[1], A. Conde[1], I. Skorvanek[2]

[1] Departamento de Física de la Materia Condensada, ICM-SE CSIC, Universidad de Sevilla, P. O. Box 1065, 41080, Sevilla, Spain

[2] Institute of Experimental Physics, Slovak Academy of Sciences, SK-040 01 Kosice, Slovakia

Abstract

The magnetic anisotropy field distribution is discussed for Hitperm alloys annealed under different field conditions leading to different induced magnetic anisotropies: zero (ZF), transversal (TF), and longitudinal (LF) field annealing and compared to that of as-quenched (AQ) melt-spun amorphous ribbon. In order to accurately use the present method, the demagnetizing factor has been obtained by analyzing the field dependence of the inverse of the field derivative of the magnetization. The coherence of the analysis is supported by testing the normalization of the complete distribution of anisotropy fields. Independently of the composition, two groups can be distinguished among the studied samples: those with mainly perpendicular anisotropy field contributions (ZF and TF samples) and those with mainly longitudinal anisotropy field contributions (LF and AQ samples). Behavior of TF samples is well reproduced using Stoner-Wohlfarth model and, in the case of as-quenched amorphous samples, the anisotropy field depends almost linearly on the thickness of the ribbon.

Keywords: Soft magnetic alloys; Hitperm alloys; Magnetic field annealing; Magnetic anisotropy.

* Corresponding author: Javier S. Blázquez

e-mail: jsebas@us.es

Journal of Alloys and Compounds 658 (2016) 367-371
http://dx.doi.org/10.1016/j.jallcom.2015.10.210

1 Introduction

One decade after the discovery of the excellent soft magnetic properties in nanocrystalline Finemet alloys by Yoshizawa et al. [1], Hitperm alloys were proposed by Willard et al. [2] to extend the range of applicability of nanocrystalline alloys to higher temperatures. In fact, the ultrasoft character of these systems is achieved by averaging out the magnetocrystalline anisotropy due to magnetic coupling between the nanocrystals [3]. However, to be effective, this mechanism requires the presence of a ferromagnetic amorphous matrix [4]. Therefore, beyond the Curie temperature of the amorphous phase, T_C^{Am}, coupling is lost. In Hitperm alloys, the partial substitution of Co for Fe leads to an enhancement of T_C^{Am}, extending the maximum temperature at which the magnetic coupling between crystallites is effective for reducing the magnetocrystalline anisotropy [5].

The typical procedure to obtain a nanocrystalline alloy implies a controlled partial crystallization of a precursor amorphous alloy produced by rapid quenching methods. Crystallization requires annealing above T_C^{Am} for Finemet alloys but below T_C^{Am} for Hitperm alloys [5]. In the latter case, stabilization of domain walls occurs due to pair ordering mechanism in conventional annealing treatments and producing an unwanted magnetic hardening [6,7,8,9]. However, this problem can be overcome after annealing under magnetic fields large enough to saturate the sample [10,11,12,13,14,15].

Field annealing, as well as stress annealing and production technique (e.g. melt spinning [16]), can induce magnetic anisotropies in the samples. The induced magnetic anisotropy has been shown to be closely related with magnetoimpedance effect as it has been widely studied in stress annealed samples [17,18,19]. Barandiaran et al. [20] developed a method to obtain the distribution of anisotropy fields perpendicular to the applied field using the demagnetization $M(H)$ branch of the hysteresis curves (i.e. from saturation to remanence), where M is the magnetization and H is the magnetic field. In this model, the probability of a certain anisotropy field H_k is described as:

Journal of Alloys and Compounds 658 (2016) 367-371
http://dx.doi.org/10.1016/j.jallcom.2015.10.210

$$P\left(H_k\right) = -\frac{H}{M_S}\frac{d^2M}{dH^2} \quad (1)$$

This expression concerns the anisotropies perpendicular to the applied field, being M_S the saturation magnetization. The normalization of this probability requires that:

$$m_r + \int_0^\infty P\left(H_k\right)dH_k = 1 \quad (2)$$

Where the relative remanence, $m_r=M_r/M_S$ (M_r is the magnetization at remanence), takes into account the anisotropy contribution parallel to the applied field. This method was initially applied to describe the induced anisotropies in soft magnetic amorphous alloys [20] and later on to soft magnetic nanocrystalline alloys [21,22,23] and to other systems [24,25]. The analysis of the applicability of this method to nanocrystalline systems conclude that misalignment leads to an asymmetrical broadening of $P(H_k)$ with a shift to lower values of the field with maximum $P(H_k)$, H_{pk}, and a shift to higher values of the average of the field over the distribution, $<H_k^{dist}>$. Moreover, the presence of interactions shifts $P(H_k)$ to lower anisotropy field values [26].

In this work, the anisotropy field distribution as well as the longitudinal anisotropy are determined by applying the method developed by Barandiaran et al. to a series of Hitperm-type alloys submitted to different field annealing treatments. Both field annealing and compositional effects are discussed.

1. Experimental

Amorphous ribbons of $Fe_{78-x}Co_xNb_6B_{16-y}Cu_y$ (x=39, 60; y=0, 1) compositions were produced by melt-spinning. Thickness and width of the different ribbons are collected in table 1. 60 mm long pieces were annealed during 1 h at the DSC peak temperature of the primary crystallization process (see table 1. for the corresponding annealing temperatures and Ref. [27] for DSC results) and under three different conditions, besides the as-quenched (AQ) amorphous samples: a) zero magnetic field (ZF), b) applying a magnetic field of 20 kA/m longitudinal to the axis of the ribbon (LF) and c) applying a field of 640 kA/m transversal to the axis and in the plane

Journal of Alloys and Compounds 658 (2016) 367-371
http://dx.doi.org/10.1016/j.jallcom.2015.10.210

of the ribbon (TF). Hysteresis loops were acquired using a Forster type B-H loop tracer using flux-gate sensors. A minimum of ten hysteresis loops were recorded per sample, keeping its position inside the tracer in order to get an average experimental curve with a reduced noise to signal ratio. A vibrating sample magnetometer was used to measure the saturation magnetization. The density of the samples was 8.1 and 8.3 g/cm^3 for alloys with 39 and 60 at. % of Co, respectively.

2 Results and discussion

Figure 1 shows the inverse of the derivative dM/dH_{app} in the range from saturation to remanence for the complete set of studied samples annealed under different annealing conditions, where M is the magnetization and H_{app} is the applied field. This parameter is the inverse of the technical susceptibility, $1/\chi^*$, which is equal to the inverse of the actual magnetic susceptibility, $1/\chi$, plus the demagnetizing factor, N_D [28]. The logarithmic scale of figure 1 allows us to appreciate the constant behavior of $1/\chi^*$ at very low fields for LF samples. For each composition this value is the lowest limit of $1/\chi^*$, which corresponds to the H_{app} range where $1/\chi$ becomes negligible in comparison to N_D. Therefore, we can directly extract N_D from this analysis. As the length of all the studied samples was the same, we can assume the same value of N_D for all the samples of each composition (width and thickness are different for different compositions). The obtained values of N_D are compared in figure 2 to the theoretical ones for flat ellipsoids with the same axis ratio. Both the trend and the order of magnitude are well reproduced. Therefore, these experimentally obtained values of N_D were used to recalculate the $M(H_{app})$ curves to $M(H)$, where $H=H_{app}-N_DM$ is the internal field.

These new $M(H)$ curves were used to obtain the probability distribution of the perpendicular anisotropy $P(H_k)$ using equation (1) as well as the relative remanence, m_r, which corresponds to the probability of parallel anisotropy. It is worth mentioning that m_r is particularly sensitive to correcting the demagnetizing field effect.

Journal of Alloys and Compounds 658 (2016) 367-371
http://dx.doi.org/10.1016/j.jallcom.2015.10.210

Figure 3 shows the obtained $P(H_k)$ curves (smoothed using 5 adjacent points averaging) for the different compositions and samples studied. Using these plots and considering that the fraction m_r corresponds to the contribution with zero perpendicular anisotropy field, the average value of the anisotropy field $<H_k>$ can be obtained. When the average is only performed over the distribution, $<H_k^{dist}>$ is obtained. The average between $<H_k^{dist}>$ and the peak value of the anisotropy field, H_{pk}, can be approximated to a single effective perpendicular anisotropy field (less than 10 % error) [26]. Table 2 collects $<H_k>$ and $<H_k^{dist}>$ values for the different studied samples and, for TF and ZF samples, H_{pk} and the ratio $2<H_k>/(<H_k^{dist}>+H_{pk})$ are also shown. The latter parameter should be 1 for a completely perpendicular distribution of anisotropies and should decrease as the longitudinal anisotropies increase. Samples can be classified in two different groups: ZF and TF samples exhibit a maximum in $P(H_k)$, whereas for LF and AQ samples a continuous decrease in $P(H_k)$ is observed as field increases.

In the case of TF samples, $<H_k>$ is larger for the compositions with larger Co content (~30 %). For each Co content, it is larger for the Cu-free alloy (~13-25 %). As previously described [29], the smaller crystallites in Cu-containing alloys and the smaller magnetocrystalline anisotropy of the crystalline α-$Fe_{61}Co_{39}$ with respect to the α-$Fe_{40}Co_{60}$ phase could explain these compositional dependencies. In addition, a larger crystalline fraction in 39 % Co containing alloys could enhance the interaction between crystallites as the average distance between them decreases. This effect can also explain a decrease in the maximum of $P(H_k)$ [26].

For ZF samples, even a larger relative increase of $<H_k>$ with Co content is observed (~100 %) but the addition of Cu does not affect the average anisotropy field. In the case of LF samples $<H_k>$~200 A/m, independently of the composition. Finally, $<H_k>$ for AQ samples shows a shape dependency, increasing with the thickness of the ribbon. Extrapolation of this trend should lead to a perfect alignment for zero thickness as shown in figure 4.

Journal of Alloys and Compounds 658 (2016) 367-371
http://dx.doi.org/10.1016/j.jallcom.2015.10.210

Table 3 collects the values of the area under $P(H_k)$, A_{dist}, as well as the value of m_r for each studied sample. As described in equation (2), the sum of m_r and the integral of $P(H_k)$ must be 1. This total value, A_{total}, also appears in table 3. The alloy that shows a higher deviation from this value is that measured for the AQ sample of the Cu-free alloy with 39 % of Co (A_{total}=0.92). The explanation is that $P(H_k)$ for this sample does not reach zero in the explored field range (see Fig. 3). In all the other cases, the departure from 1 is below 4 % in spite of the high noise due to numerical derivation.

An apparent distribution of magnetic anisotropy fields can also be obtained even for a single anisotropy field when the easy axis does not form 90º with respect to the applied field [20] or, more generally, if there is an angular distribution of easy axis [26]. Therefore, $P(h_k)$ curves were simulated assuming sets of Stoner-Wohlfarth regions with different angular distributions of the easy axis around a perpendicular orientation ($TF^{S\text{-}W}$) to the applied field, where $h_k=H/H_k$. In fact, in all these simulated results, the capital H will be substituted by a lowercase h to indicate that we refer to a relative field (without units) being h_k=1 the value of the anisotropy field, identical for each particle of the set.

As angular distribution broadens, $P(h_k)$ also broadens starting from a Dirac delta function for a perfect perpendicular alignment. Moreover, whereas the average value of the anisotropy field $<h_k>$ and the peak value, h_{pk}, shift to lower values, $<h_k^{dist}>$ shifts to higher values as previously discussed [26]. Figure 5 shows, as a function of the broadening of the angular distribution, the area under $P(h_k)$ curves along with m_r and $<h_k>$ obtained for $TF^{S\text{-}W}$ from Stoner-Wohlfarth model.

As stated above, our samples can be classified in two different groups: TF and ZF samples, with the local magnetic anisotropy axes oriented predominantly perpendicular to the applied field; and AQ and LF samples, with the local magnetic anisotropy axes oriented predominantly parallel to the applied field. In order to compare the experimental data to the simulated ones, relative field parameters were obtained after dividing by $(<H_k^{dist}>+H_{pk})/2$.

Journal of Alloys and Compounds 658 (2016) 367-371
http://dx.doi.org/10.1016/j.jallcom.2015.10.210

The corresponding experimental values of m_r for TF samples indicate an angular broadening of ~1-2 degrees, which is in agreement with the clear perpendicular domain pattern observed by MOKE in these alloys [30]. The experimental values of $<h_k>$ (see table 2) are close to 1 for these samples, also in agreement with the expected values from Stoner-Wohlfarth model for such a small broadening of the angular distribution as shown in figure 5.

4 Conclusions

The magnetic anisotropy field distribution is obtained after correcting the demagnetizing factor and taking into account two contributions: perpendicular to the applied field and parallel to it. The former contribution is obtained as a probability distribution of anisotropy fields, $P(H_k)$, from the second derivative of the demagnetization curve and the latter contribution is estimated from the reduced remanence, m_r. This analysis has been applied to four Hitperm $Fe_{39-x}Co_{39+x}Nb_6B_{16-y}Cu_y$ (x=0, 21; y=0, 1) alloys obtained by melt-spinning in the amorphous as-quenched state (AQ) as well as nanocrystallized under zero magnetic field (ZF), under a magnetic field longitudinal to the axis of the ribbon (LF) and under a magnetic field in the plane of the ribbon but transversal to its axis (TF). Two groups can be distinguished among the studied samples: those with mainly perpendicular anisotropy field contributions (TF and ZF) and those with mainly longitudinal anisotropy field contributions (AQ and LF). The behavior of TF samples can be well reproduced using a Stoner-Wohlfarth model and, in the case of AQ samples, the anisotropy field grows almost linearly with the thickness of the ribbon.

Acknowledgements: Work supported by the Spanish MINECO and EU FEDER (Project MAT 2013-45165-P), the PAI of the Regional Government of Andalucía and the Slovak projects APVV-0492-11, VEGA 2/0192/13. The Slovak team acknowledges also the support of the

Journal of Alloys and Compounds 658 (2016) 367-371
http://dx.doi.org/10.1016/j.jallcom.2015.10.210

Operational Program “Research and Development” financed through European Regional

Development Fund through the projects ITMS 26220120019 and ITMS 26220220061.

References

[1] Y. Yoshizawa, S. Oguma, K. Yamauchi, J. Appl. Phys. 64 (1988) 6044.
[2] M. A. Willard, D. E. Laughlin, M. E. McHenry, D. Thoma, K. Sickafus, J. O. Cross, V. G. Harris, J. Appl. Phys. 84 (1998) 6773.
[3] G. Herzer, IEEE Trans. Magn. 25 (1989) 3327.
[4] A. Hernando, M. Vázquez, T. Kulik, C. Prados, Phys. Rev. B 51 (1995) 3581.
[5] M. E. McHenry, M. A. Willard, D. E. Laughlin, Progress Mater. Sci. 44 (1999) 291.
[6] J. S. Blázquez, V. Franco, A. Conde, J. Phys.: Cond. Matter 14 (2002) 11717
[7] T. Kulik, J. Ferenc, A. Kolano-Burian, X.B. Liang, M. Kowalczyk, J. All. Compd. 434 (2007) 623
[8] M. A. Willard, M. Daniil, K. E. Kniping, Scripta Mater. 67 (2012) 554
[9] Zs. Gercsi, F. Mazaleyrat, L. K. Varga, J. Magn. Magn. Mat. 302 (2006) 454
[10] I. Skorvanek, J. Marcin, T. Krenicky, J. Kovac, P. Svec, D. Janickovic, J. Mag. Mag. Mat. 304 (2006) 203
[11] I. Skorvanek, J. Marcin, J. Turcanova, M. Wojcik, K. Nesteruk, D. Janickovic, P. Svec, J. Mag. Mag. Mat. 310 (2007) 2494
[12] I. Skorvanek, J. Marcin, J. Turcanova, J. Kovac, P. Svec, J. All. Compd. 504S (2010) S135
[13] I. Skorvanek, J. Marcin, M. Capik, M. Varga, J. Turcanova, J. Kovac, P. Svec, D. Janickovic, F. Kovac, V. Stoyka, Magnetohydrodynamics 48 (2012) 371
[14] F. Johnson, H. Garmestani, S. Y. Chu, M. E. McHenry, and D. E. Laughlin, IEEE Trans. Mag. 40 (2004) 2697
[15] K. Suzuki, N. Ito, J. S. Garitaonandia, J. D. Cashion, G. Herzer, J. Non-Cryst. Sol. 354 (2008) 5089
[16] M. Tejedor, B. Hernando, J. Phys. D: Appl. Phys. 13 (1980) 1709
[17] M. Vázquez, G. V. Kurlyandskaya, J. M. García-Beneytez, J. P. Sinnecker, J. M. Barandiarán, V. A. Lukshina, A. P. Potapov, IEEE Trans. Mag. 35 (1999) 3558.
[18] G. V. Kurlyandskaya, J. M. Barandiarán, M. Vázquez, D. García, N. V. Dmitrieva, J. Mag. Mag. Mat. 215-216 (2000) 740.
[19] J. L. Muñoz, G. V. Kurlyandskaya, J. M. Barandiarán, A. P. Potapov, M. Vázquez, Mat. Sci. Forum 373-376 (2001) 269.
[20] J. M. Barandiarán, M. Vázquez, A. Hernando, J. González, G- Rivero, IEEE Trans. Magn. 25 (1989) 3330
[21] V. Franco, C. F. Conde, A. Conde, J. Magn. Magn. Mat. 185 (1998) 353
[22] V. Franco, C. F. Conde, A. Conde, J. Appl. Phys. 84 (1998) 5108
[23] S. S. Modak, F. Mazaleyrat, M. Lo Bue, L. K. Varga, S. N. Kane, Sol. State Phys. AIP Conf. Proc. 1447 (2012) 1163
[24] G. Bottoni, D. Candolfo, A. Cecchetti, J. Appl. Phys. 81 (1997) 3794
[25] V. Dubuget, S. Dubourg, P. Thibaudeau, F. Duverger, IEEE Trans. Magn. 46 (2010) 1139
[26] V. Franco, A. Conde, Appl. Phys. Lett. 74 (1999) 3875
[27] J.S. Blázquez, C.F. Conde, A. Conde, J. Non-Cryst. Sol. 287 (2001) 187
[28] H. Zijlstra, Experimental Methods in Magnetism. 2. Measurement of Magnetic Quantities, North Holland Publishing Company, Amsterdam, 1967, p.138.
[29] J. S. Blázquez, J. Marcin, M. Varga, V. Franco, A. Conde, I. Skorvanek, J. Appl. Phys. 117 (2015) 17A301
[30] J. S. Blázquez, J. Marcin, F. Andrejka, V. Franco, A. Conde, I. Skorvanek, presented at ICM2015

Journal of Alloys and Compounds 658 (2016) 367-371
http://dx.doi.org/10.1016/j.jallcom.2015.10.210

Table 1.

Width and thickness of the different ribbons used in this study

Composition	Annealing temperature (K) [27]	Width (mm) ±0.05	Thickness (μm)
$Fe_{18}Co_{60}Nb_6B_{15}Cu_1$	736	4.75	26.7±0.4
$Fe_{18}Co_{60}Nb_6B_{16}$	748	5.00	18.3±0.3
$Fe_{39}Co_{39}Nb_6B_{15}Cu_1$	739	4.75	26.3±0.5
$Fe_{39}Co_{39}Nb_6B_{16}$	766	4.40	30.0±0.4

Table 2

Average anisotropy field, $<H_k>$, average of the anisotropy field over the distribution, $<H_k^{dist}>$, anisotropy field at the peak of the distribution, H_{pk}, and relative average of the anisotropy field.

Composition		$<H_k>$ A/m	$<H_k^{dist}>$ A/m	H_{pk} A/m	$2<H_k>/(<H_k^{dist}>+H_{pk})$
$Fe_{18}Co_{60}Nb_6B_{15}Cu_1$	AQ	865	1170		
	ZF	1425	1830	1650	0.82
	TF	1955	2040	1810	1.02
	LF	190	760		
$Fe_{18}Co_{60}Nb_6B_{16}$	AQ	705	1040		
	ZF	1415	2020	1575	0.79
	TF	2235	2330	2000	1.03
	LF	210	720		
$Fe_{39}Co_{39}Nb_6B_{15}Cu_1$	AQ	940	1220		
	ZF	815	1120	800	0.85
	TF	1400	1430	1200	1.06
	LF	185	690		
$Fe_{39}Co_{39}Nb_6B_{16}$	AQ	1255	1820		
	ZF	795	1140	790	0.82
	TF	1795	1830	1575	1.05
	LF	190	730		

Journal of Alloys and Compounds 658 (2016) 367-371
http://dx.doi.org/10.1016/j.jallcom.2015.10.210

Table 3

Area under $P(H_k)$, relative remanence and sum of these two parameters.

Composition		A_{dist}	m_r	A_{total}
$Fe_{18}Co_{60}Nb_6B_{15}Cu_1$	AQ	0.74	0.25	0.99
	ZF	0.78	0.20	0.98
	TF	0.96	0.01	0.97
	LF	0.25	0.74	0.99
$Fe_{18}Co_{60}Nb_6B_{16}$	AQ	0.68	0.28	0.97
	ZF	0.70	0.27	0.97
	TF	0.96	0.01	0.97
	LF	0.29	0.71	1.00
$Fe_{39}Co_{39}Nb_6B_{15}Cu_1$	AQ	0.77	0.21	0.98
	ZF	0.73	0.27	1.00
	TF	0.98	0.02	1.00
	LF	0.27	0.72	0.99
$Fe_{39}Co_{39}Nb_6B_{16}$	AQ	0.69	0.23	0.92
	ZF	0.70	0.29	0.98
	TF	0.98	0.01	0.99
	LF	0.26	0.73	0.99

Journal of Alloys and Compounds 658 (2016) 367-371
http://dx.doi.org/10.1016/j.jallcom.2015.10.210

Figure captions

Figure 1. Inverse of the technical susceptibility for all the studied samples.

Figure 2. Experimental demagnetizing factors vs. theoretical ones for a flat ellipsoid with the same axis ratio.

Figure 3. Distribution of the anisotropy fields perpendicular to the applied field for all the studied samples.

Figure 4. Average anisotropy field for the different as-quenched samples as a function of the thickness of the ribbon.

Figure 5. Area under $P(h_k)$ curves along with m_r and $\langle h_k \rangle$ obtained as a function of the broadening of an angular distribution of the easy axis of Stoner-Wohlfarth particles around 90º with respect to the applied field.

Journal of Alloys and Compounds 658 (2016) 367-371
http://dx.doi.org/10.1016/j.jallcom.2015.10.210

Figure 1

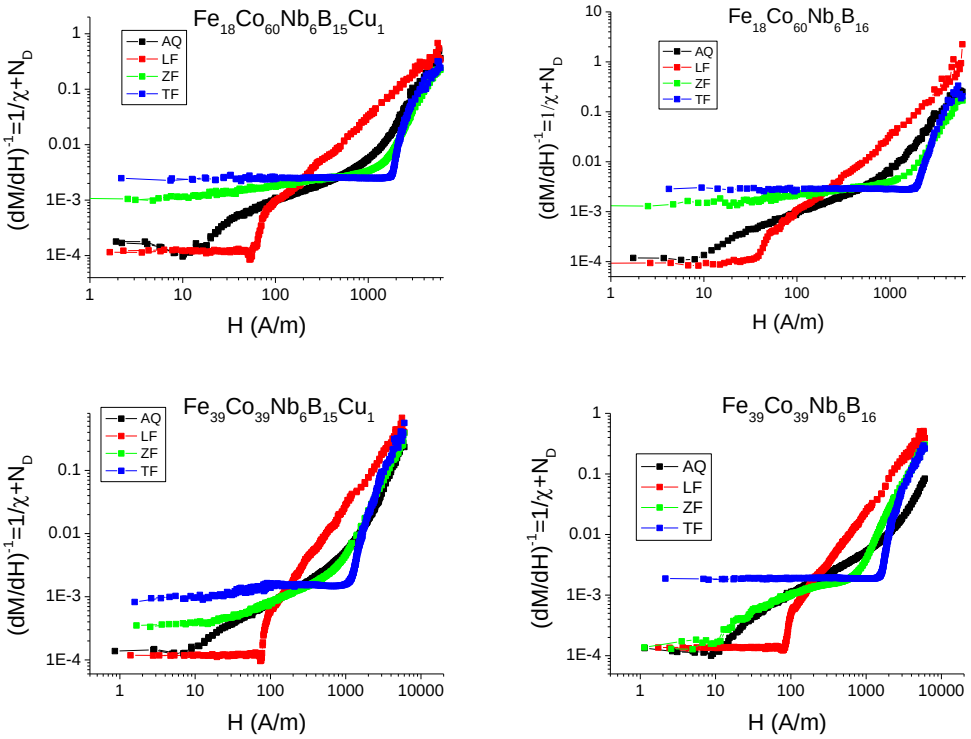

Journal of Alloys and Compounds 658 (2016) 367-371
http://dx.doi.org/10.1016/j.jallcom.2015.10.210

Figure 2

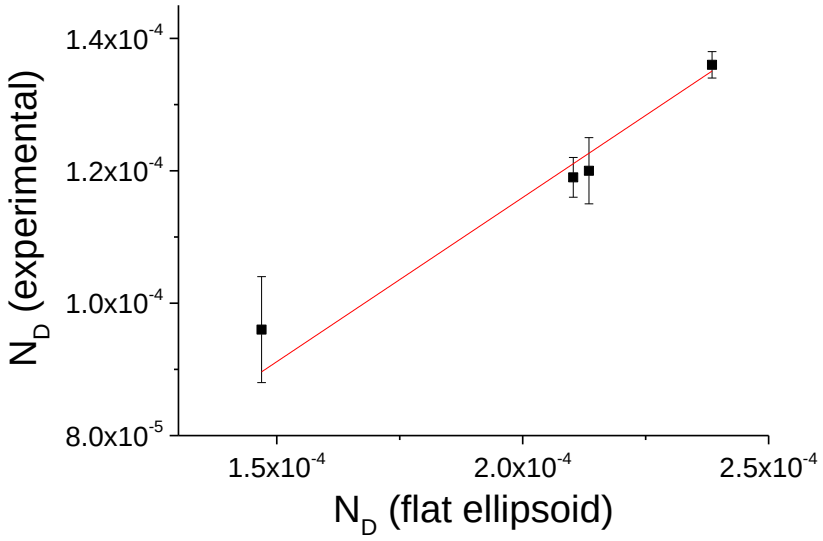

Journal of Alloys and Compounds 658 (2016) 367-371
http://dx.doi.org/10.1016/j.jallcom.2015.10.210

Figure 3

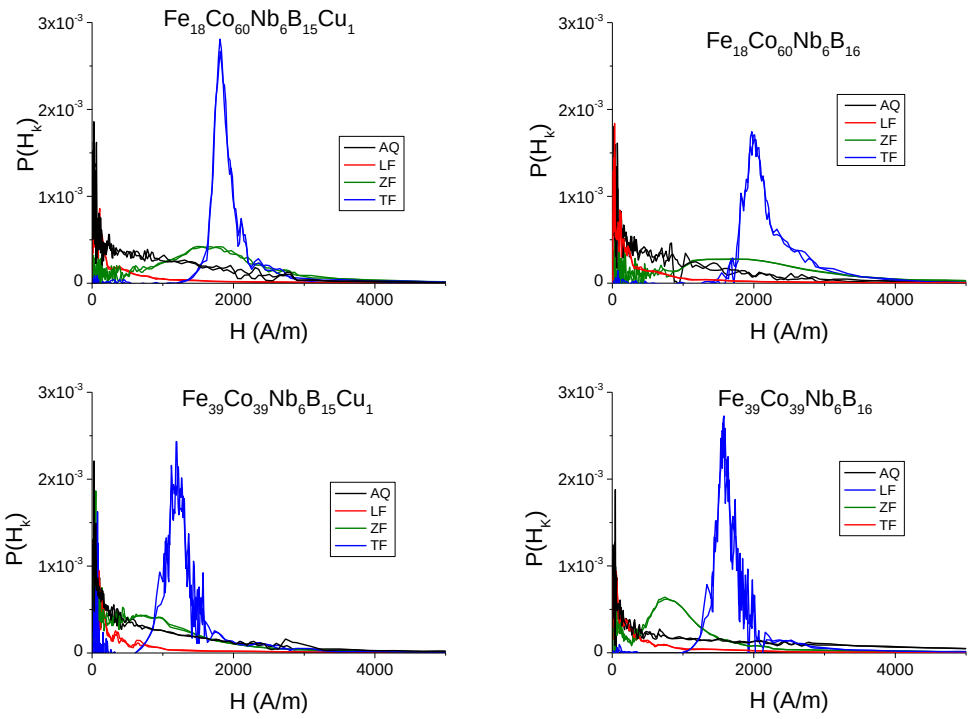

Journal of Alloys and Compounds 658 (2016) 367-371
http://dx.doi.org/10.1016/j.jallcom.2015.10.210

Figure 4

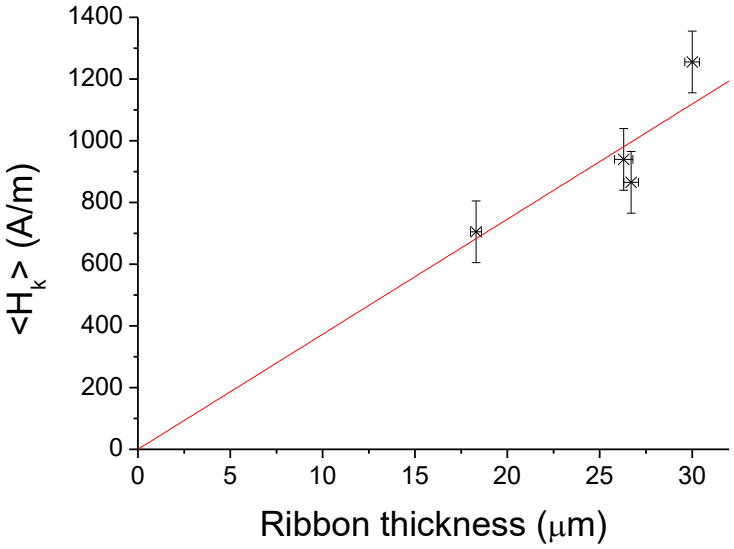

Journal of Alloys and Compounds 658 (2016) 367-371
http://dx.doi.org/10.1016/j.jallcom.2015.10.210

Figure 5